A Higher Order Lateral Mode Suppression Scheme for Terahertz Quantum Cascade Laser Waveguides

Huda Tanvir, *Student Member, IEEE,* B.M.A Rahman, *Senior Member, IEEE,* and K.T.V Grattan

***Abstract*—The modal performance of a slot-clad metal-metal waveguide for terahertz quantum cascade lasers is elucidated in this work. Terahertz quantum cascade lasers, based on metal-metal waveguides having a large ridge width, are susceptible to lase with higher-order lateral modes which may produce poor quality beams and can lead to detrimental consequences for certain applications. By comparing the modal performance of the slot-clad waveguide with previously reported designs, it has been shown that the slot clad metal-metal waveguide can significantly enhance the degree of suppression of higher order lateral modes.**

***Index Terms*—Numerical approximation and analysis, Terahertz, Semiconductor lasers, Quantum cascade.**

I. Introduction

THE quest to harness the full potential of quantum cascade lasers (QCLs) as an important source of terahertz (THz) radiation has triggered a flurry of research activity in semiconductor and solid state physics in recent years. Several breakthroughs has been achieved in optimizing the performance of the device since the first demonstration a THz QCL [1] in 2002. Most notable amongst these achievements was the demonstration of a resonant phonon based THz QCL on a metal-metal waveguide [2]. A waveguide is a crucial part of any laser device and for THz lasers, designing a low-loss waveguide is a critical part of the design phase as the absorption of the materials (at these wavelengths) tends to rise by a factor given by λ^2 (where λ is the operating wavelength). For THz QCL's two of the most commonly used waveguides are the semi-insulating [3], [4] and metal-metal [2] waveguides. Metal-metal waveguides based THz QCL's have so far outperformed semi insulating (SI) waveguide based devices as QCL's with metal-metal waveguides can operate at higher temperatures and require low threshold current densities [5].

Unfortunately, due to the sub-wavelength dimension of the waveguide and the high facet reflectivity of the device, metal-metal waveguide based THz QCL's produce highly divergent far-field beam patterns [6]. This often leads to poor out coupling of the emitted radiation from the facet of the device. In order to achieve a narrow beam angle and improve the radiation out-coupling in a metal-metal waveguide THz QCL, a wide ridge geometry may be used. However, it is well known that wider ridge waveguides are susceptible to lase with higher-order lateral modes, as the threshold gain of the fundamental (TM^{00}) and higher-order lateral (TM^{0n}) modes are very similar. This results in the appearance of multiple lobes in the far-field pattern of the lasing mode [7], [8]. Whilst it may well be insignificant for certain applications (such as super heterodyne detection and spectroscopy), for other areas such as imaging where a clean far-field profile of the source is critical, such an effect could have detrimental consequences. To address this problem, surface emitting devices have been proposed as a solution as they are able to achieve lasing with a single mode [9]. However, due to complex fabrication techniques involved with surface emitting QCL's, edge-emitting are often preferred over surface emitting devices.

To address the challenge of improving the beam quality of an edge emitting THz QCL based on a metal-metal waveguide, several proposals have been made over the past few years. One such was to fabricate a silicon micro-lens at the facet of the device [10]. The device reported demonstrated upto 5 fold rise in output power with a considerably narrow beam angle (FWHM$\sim 4.8^{\circ}$), however, the positioning of the lens and its precise alignment at the facet of the device proved be to a challenging task [10]. More recently, Fan *et al.* demonstrated a wide-ridge metal-metal THz QCL [7] incorporating an exposed region of the top n^+-GaAs layer, aimed at suppressing the mode competition arising from the higher-order lateral modes. The waveguide fabricated with a narrower metal cladding layer demonstrated a reasonable rise in the threshold gain (g^{th}) of the higher order modes whilst maintaining a lower g^{th} for the fundamental mode. Complementary to that has been the report of a side absorber guide with a central slot that favours lasing with TM^{01} mode [11].

In this article an alternative approach to control the lasing mode in a wide ridge metal-metal waveguide for THz QCL (based on GaAs/AlGaAs material system) has been demonstrated. It is shown that by using a slot-clad metal-metal waveguide, the modal losses of the higher order modes can be raised by as much as 4-fold, compare to a conventional device or by more than 2 fold compared to the side absorber design [7]. This has been achieved with only a negligible rise in the loss value of the fundamental mode.

II. Device structure

The slot-clad waveguide structure reported here is schematically shown in Fig. 1. In this structure, the slotted regions in the upper metal cladding layer were placed W_1 μm away from the lateral edges of the QCL cavity. The width of the slotted region was considered to be kept constant at $\delta = 3.0$ μm and the waveguide width (W) with this arrangement was defined as $W = W_2 + 2W_1 + 2\delta$. The refractive indices

The authors are with the School of Engineering and Mathematical Sciences, City University London, Northampton Square, London EC1V 0HB, United Kingdom. E-mail: (huda.tanvir.1@city.ac.uk).

Manuscript received April 01, 2012

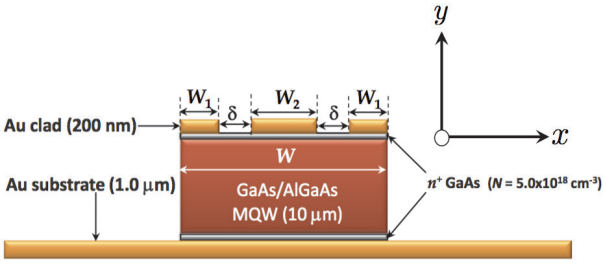

Fig. 1. Schematic cross-sectional view of the slot-clad metal-metal waveguide for a THz QCL.

of the upper and lower n^+ GaAs layers were calculated (using the Drude-Lorentz model [12]) to be $5.93 + j23.32$ for a carrier concentration of $N = 5.0 \times 10^{18}\text{cm}^{-3}$ at the operating wavelength of $\lambda = 100$ μm. The thicknesses of these two layers were taken as 50 and 75 nm, respectively. The thicknesses of the upper and lower Au layers were taken to be 200 nm and 1.0 μm, respectively. The refractive index of the Au layers were taken as $240 + j400$ at $\lambda = 100$ μm [13]. The 10 μm thick active region was considered to have a complex refractive index of $3.49 + j0.0061$ [7]. In order to reveal the characteristics of the waveguide, the structure was simulated using a rigorous full vectorial **H**-field based finite element method [14], [15]. The operating frequency of the structure was considered to be 3.0 THz. To asses the effect of the exposed n-doped GaAs region above the active layer, the position of the slotted region was varied by increasing the width of the outer metal layer (W_1) and decreasing the width of the inner metal layer (W_2), thereby keeping the width of the waveguide ridge constant at 200 μm. The width of the slotted opening regions were also kept constant at $\delta = 3.0$ μm, although this parameter can also be optimized as necessary.

III. Evaluation of Performance

The performance of the QCL was evaluated using the conventional figure of merit, g^{th} which is the threshold gain where $g^{th} = \frac{\alpha_w + \alpha_m}{\Gamma}$, and α_w is the waveguide loss, α_m is the mirror loss and Γ is the confinement factor of the lasing mode in the QCL cavity which can be derived from the Poynting vector relation [15]. The waveguide loss was calculated from the imaginary part of the complex propagation constant,γ, of the lasing mode and can be defined as $\alpha_w = 2\Im(\gamma)$. For highly confined modes of a QCL, mirror losses can often be neglected from the calculation of the g^{th} parameters since in metal-metal waveguides $\alpha_w \gg \alpha_m$ due to high facet reflectivity of the modes. However, the calculation of the facet reflectivity is critical, particularly when the slope efficiencies are considered. Nevertheless, for the analysis presented here, the contribution from the mirror loss has been neglected as the focus of the discussion is on raising the waveguide loss of the higher-order lateral modes. The effect of varying W_1 on the critical parameters of the lasing modes, such as the threshold gain (g^{th}), the effective index, the confinement factor Γ were analysed rigorously.

IV. Results

A. Impact on effective index

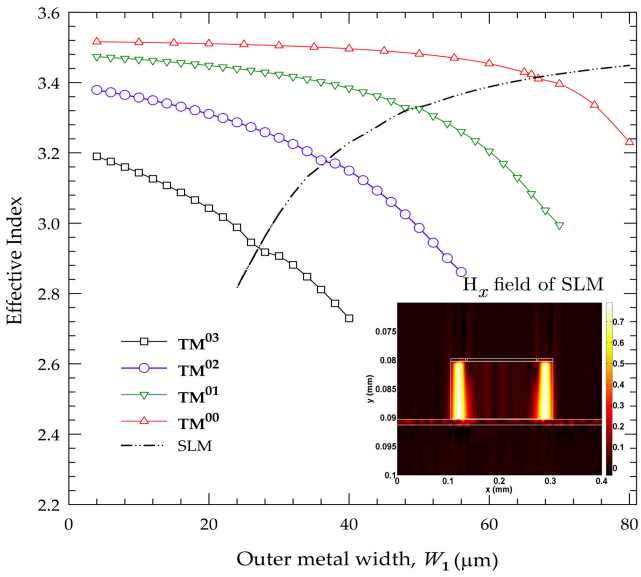

Fig. 2. Variation in the effective index of the fundamental and higher-order lateral modes as W_1 was varied.

The variation in effective indices of the fundamental (TM^{00}) and higher-order lateral (TM^{01}, TM^{02} and TM^{03}) modes as a function of W_1 is shown in Fig. 2. A strong functional response was observed for the effective indices of the higher order modes as W_1 was varied. However, for the fundamental TM^{00} mode, the variation in the effective index as a function of W_1 was observed to be far less pronounced. This can be attributed to the fact that the propagation properties of the lasing modes in this slot-clad waveguide are primarily controlled by the central metal layer, of width W_2. As W_1 was increased, W_2, was reduced to maintain a constant ridge width and W_2 starts to match the cut-off width of the higher order modes in a conventional metal-metal waveguide. Thus it can be inferred that reducing W_2 has similar effect on the properties of the modes as reducing the width of the waveguide has in a conventional metal-metal waveguide [12]. It can also be observed that the higher order modes are highly dispersive, having a sharply varying effective index profile with increasing W_1 (decreasing W_2), whereas the fundamental mode hardly has any such noticeable dispersive features. At a sufficiently large W_1, the waveguide can also support a side lobe mode (SLM) whose effective index variation and intensity profile are shown (as an inset) in Fig. 2. It can be observed that as W_1 increases, the effective index of the SLM increases whilst the effective indices of the central TM^{0n} modes reduce. This results in possible phase matching between the SLM and the TM^{0n} modes which can be seen to a cause slight perturbation in the effective index profiles of these TM^{0n} modes. The SLM was observed to be in phase synchronism with the TM^{03} mode at $W_1 \sim 28$ μm, with the TM^{02} mode at $W_1 \sim 36$ μm and with the TM^{01} mode at $W_1 \sim 50$ μm, respectively. Phase matching was also observed between the SLM and the fundamental TM^{00} mode; however, the

resultant perturbation in the effective index profile of the TM^{00} mode was infinitesimal and hence not noticeable in Fig. 2. To investigate further the effect of mode coupling between the SLM and the lateral modes, the mode profiles of the latter were also analyzed in this study.

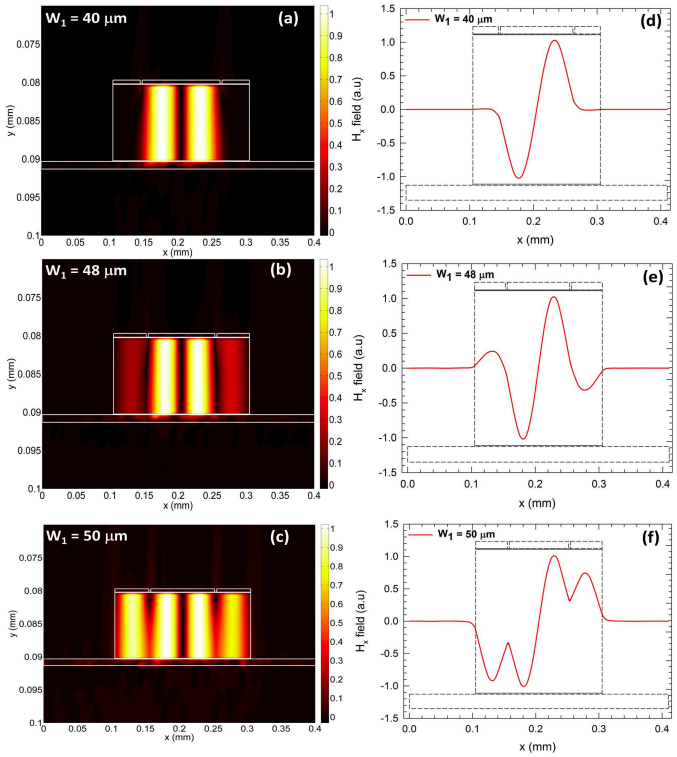

Fig. 3. Variation of the power intensity (calculated from the poynting vector relation [15]) of the TM^{01} mode along the transverse directions at $W_1 = 40, 48$ and 50 μm are shown in parts (a), (b) and (c) of the figure. The corresponding variation of the H_x field of this mode along x-axis (at the centre of the ridge) are shown in parts (d), (e) and (f) of the figure.

Figure 3 shows the H_x field profiles of the TM^{01} mode, particularly when this mode interacts with the SLM mode. Away from the influence of the SLM (for W_1 <<50 μm), the mode clearly shows two peak values at $W_1 = 40$ μm, as illustrated in Fig. 3 (a). The TM^{01} mode is being supported by the central metal layer (of width W_2) and is strongly localised at the center of the active region with a highly symmetric power distribution along the vertical direction. Variation of the H_x field along the x- direction is shown in Fig. 3(d) for $W_1 = 40$ μm from which it can be clearly seen that the field distribution is highly asymmetric having two peaks with a single zero crossing. As the W_1 increases, the effective index of the TM^{01} mode decreases at the same time when the effective index of the SLM increases (shown earlier in Fig. 2). As a result the TM^{01} mode begins to couple with the SLM and slowly starts to resemble features of the latter. This is shown in the power intensity distribution in Fig. 3(b) for $W_1 = 48$ μm from where the profile can be seen to have two lobes being supported by the central metal layer. From this figure, the mode can also be seen to have side lobes supported by the outer metal layer which is one of the key modal characteristics of the SLM (which was shown earlier in Fig.2). As the coupling between the SLM and the TM^{01} mode is still weak (at this value of W_1) the side lobes of the resultant mode can be seen to be less intense than the central lobes. Analyzing the H_x field variation of the mode along the horizontal axis in Fig. 3 (e), it can be further observed that the resultant mode resembles the characteristic feature of a supermode having four field peaks and three zero crossings. It is important to mention here that the intensity profiles shown here does not resemble a TM^{03} mode which would consistently have three zero crossing supported by the central metal layer. The mode shown here is a TM^{01} mode which resembles a complex field profile due to coupling between the TM^{01} mode and the SLM. In addition to that, the dispersion profile shown earlier in Fig. 2 suggests that the TM^{03} mode cannot be supported for W_1>48 μm (since the width of the central metal layer W_2 is below the cut-off width for the TM^{03} mode). At the point of maximum coupling of the TM^{01} mode with the SLM i.e. at $W_1 = 50$ μm, a subtle change in mode profile can be observed from Fig. 3 (c) where the variation of the power intensity profile is shown. The field lobes supported by the outer metal layer can be seen to have relatively higher intensity than was observed previously at $W_1 = 48$ μm. It can also be observed that the resultant mode has a dip in the field near the upper cladding region. This can be clearly seen to be influenced by the 3.0 μm slotted openings at the upper metal layer which exposes the n^+ GaAs layer above the active region. The mode can also be seen to have a considerable overlap of the field into the lower metal cladding layer which greatly influences the modal loss. This coupled supermode can also be further examined from the variation of the H_x field of the mode along the horizontal direction, shown in Fig. 3 (f) at $W_1 = 50$ μm. It can be seen that the amplitude of the side lobes increases substantially as the coupling between the SLM and the TM^{01} strengthens further, due to pronounced phase matching. The resultant coupled supermode can be seen to have four intense field maxima but with a single zero crossing lying at the centre of the waveguide. However, unlike previously (at $W_1 = 48$ μm), the resultant mode can be seen to have a single zero crossing which confirms the fact that although the mode is highly coupled, it still strongly resembles the key features of a first order TM^{01} mode. Although it is necessary to analyse the mode profiles whilst assessing the performance of a QCL waveguide, it is even more critical to analyze the crucial performance defining parameters of the device such as the waveguide loss, optical confinement and the threshold gain of the lasing modes.

B. Impact on waveguide loss

The variations in the modal loss (α_w) of the fundamental and higher order lateral modes as a function of the outer metal width W_1 are shown in Fig. 4. The loss value (α_w) of the fundamental TM^{01} mode can be observed to increase slowly as W_1 is increased for W_1< 40 μm. However, for W_1>40 μm, α_w can be seen to rise with an increasing gradient for this mode as the width of the central metal layer, W_2, reduces. For W_1<40 μm the inner metal width W_2 is sufficiently large ($W_2 \sim 114$ μm, which is substantially higher than the cut-off width of the mode in a conventional edge emitting metal-metal waveguide) to support a low loss TM^{00} mode. As a

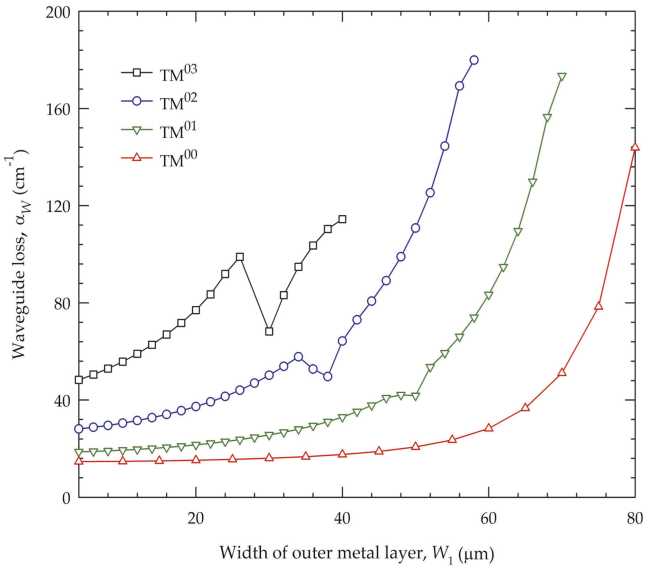

Fig. 4. Variation in waveguide loss of the fundamental and lateral higher order mode as a function of the width of the outer metal layer W_1

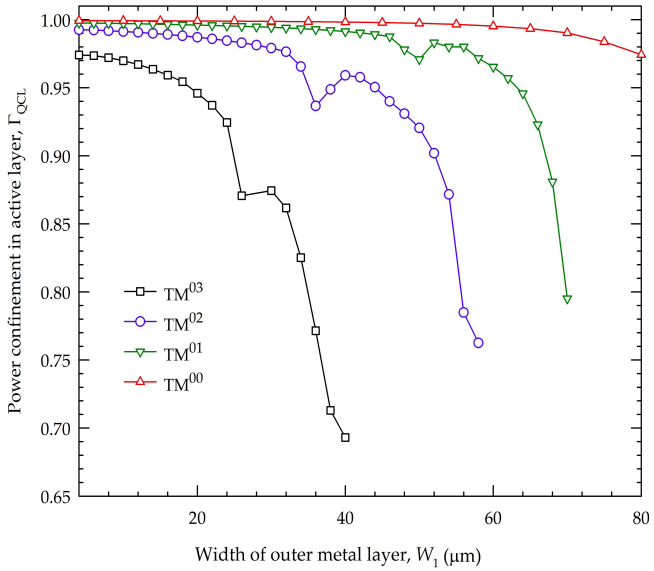

Fig. 5. Variation in power confinement in active layer of the fundamental and lateral higher order modes as a function of the width of the outer metal layer, W_1.

result no noticeable variation in α_w can be seen for W_1<40 μm, whereas above 40 μm, α_w can be seen to rise steeply as the value of W_2 approaches the value of cut-off waveguide width of the mode. Similar observations can also be made for the higher-order lateral modes; however, a faster rise in α_w was observed for these higher-order modes. It can also be observed that the relative magnitude of α_w of the higher order modes is substantially larger than the magnitude of α_w of the fundamental mode. Perturbation in the α_w profiles can be observed for the higher order modes which is due to pronounced inter-modal interaction between the higher order modes and the SLM when the two modes are phase matched. For the TM^{01} mode, a slight perturbation can be observed in the α_w profile at $W_1 \sim 44$ μm which arises due to phase synchronism with the SLM (which was shown previously in Fig. 2). For the TM^{02} and TM^{03} modes the discontinuities in their α_w profiles were noticed to be much higher due to stronger interaction of its phase velocity with that of the SLM. It can be observed here that the interaction between the SLM and the fundamental TM^{00} mode resulted in negligible change in α_w of the TM^{00} mode.

C. Impact on power confinement

The variation in the power confinement in the active layer (Γ_{QCL}) of the fundamental and higher order modes as a function of W_1 are shown in Fig. 5. The smallest variation in Γ_{QCL} (with respect to W_1) can be observed for the fundamental TM^{00} mode. As W_1 was increased, the width of the inner metal layer remained sufficiently large to support the TM^{00} mode without causing any significant change in the modal field. As such the mode maintains a symmetric overlap inside the active region of the device. For the higher-order lateral modes, however, the situation is different. For these modes, an increasing W_1 results in a faster drop in Γ_{QCL} as these modes are forced to reach their cut-off point. A small perturbation can be observed in the Γ_{QCL} profiles of the higher order modes at such values of W_1 where phase matching with the SLM occurs with the higher-order lateral modes. It is interesting that the Γ_{QCL} value for the SLM was observed to rise with increasing W_1; however, this is not shown here (in Fig. 5).

D. Impact on threshold gain

The rise in the waveguide loss and a drop in power confinement of the lasing modes will undoubtedly have a profound impact on the threshold gain (g^{th}) values. This can be seen by analyzing the variation in g^{th} of the TM modes and the side lobe mode (SLM) as a function of W_1 which is shown in Fig. 6.

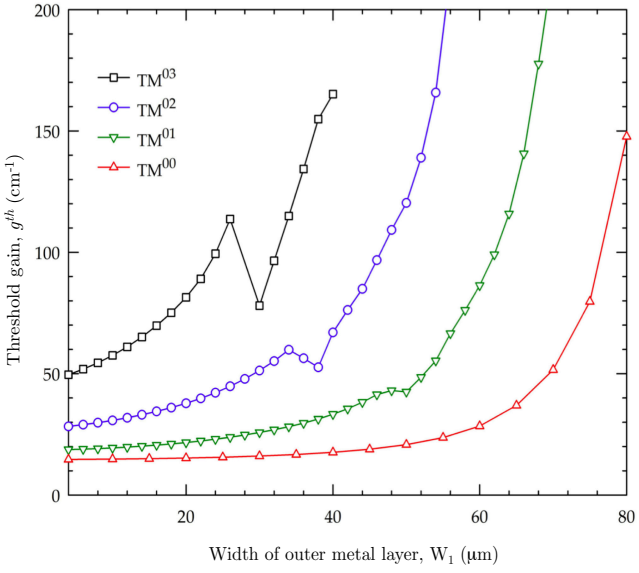

Fig. 6. Variation in threshold gain (g^{th}) of the fundamental and lateral higher order mode as a function of the width of the outer metal layer W_1

At a low value of W_1, the fundamental mode can be seen to have the lowest threshold gain. In fact the g^{th} value of this mode can be seen to remain nearly unchanged even for higher values of W_1. A very modest rise in g^{th} of the TM^{00} mode can be observed as W_1 was varied between $40-60$ μm. Above 60 μm, the g^{th} value was observed to rise exponentially. The TM^{01} mode was seen to have a slightly higher lasing threshold than the fundamental TM^{00} mode when $W_1 \sim 0$. However, upon increasing W_1, the g^{th} value of the TM^{01} mode can be seen to rise faster, thus increasing the differential threshold gain Δg^{th} between the TM^{00} and TM^{01} modes. Due to the coupling between the SLM and the TM^{01} modes, a slight drop in g^{th} can be observed at around $W_1 \sim 56$ μm. Beyond this value of W_1, an exponential rise in g^{th} can be observed for the TM^{01} mode. The TM^{02} mode was noticed to have a higher g^{th} value than the TM^{01} mode which also gives a higher Δg^{th} between the TM^{00} and the TM^{02} modes. The rate of rise in g^{th} of the TM^{02} mode was noticed to be much faster than that of the first order mode. A drop in g^{th} value can be observed at $W_1 = 36$ μm when the TM^{02} mode is strongly phase matched with the SLM. A nearly exponential rise in g^{th} value can be observed for this mode as W_2 becomes smaller and this mode slowly reaches its cut-off point. The differential threshold gain between the TM^{00} and TM^{03} mode was noticed to be the highest, due to a steep rise in the g^{th} value of the TM^{03} mode. A sharp fall in the lasing threshold of the TM^{03} mode can be observed due to its coupling with the SLM. Beyond $W_1 = 32$ μm, a steep rise in g^{th} value can be seen before W_2 becomes sufficiently small and the mode reaches its cut-off point. On the other hand, the threshold gain of the SLM was noticed to decrease exponentially as W_1 was increased. However, this is not shown here in the figure.

V. Comparison with existing waveguides

In order to assess the scale mode suppression achievable in the slot waveguide presented here with that of a narrow-clad waveguide, a comparison needs to be performed in the threshold gain of the fundamental and lateral higher order modes. This is analysed by comparing the threshold gain values of the fundamental and higher-order lateral modes obtained by performing a modal analysis of a slot-clad metal-metal waveguide, the narrow clad metal-metal waveguide [7] and a conventional metal-metal waveguide. Such a comparison is shown in Fig. 7.

A comparison between the threshold gain values of the fundamental and lateral higher order modes is shown in Fig. 7. The solid circles in Fig. 7 show, the g^{th} values of the fundamental and higher order modes in a conventional edge emitting THz QCL waveguide. The solid squares denotes the g^{th} values of the modes in a narrow clad waveguide, whereas the solid triangles shows the g^{th} values of the modes in a slot clad waveguide. The schematic representation of these three structures are also included here (as insets for reference). It can observed that the fundamental mode remains essentially unaffected as the geometry of the upper metal layer was varied. However, the differential threshold gain, Δg^{th}, between the fundamental and higher order modes can be seen

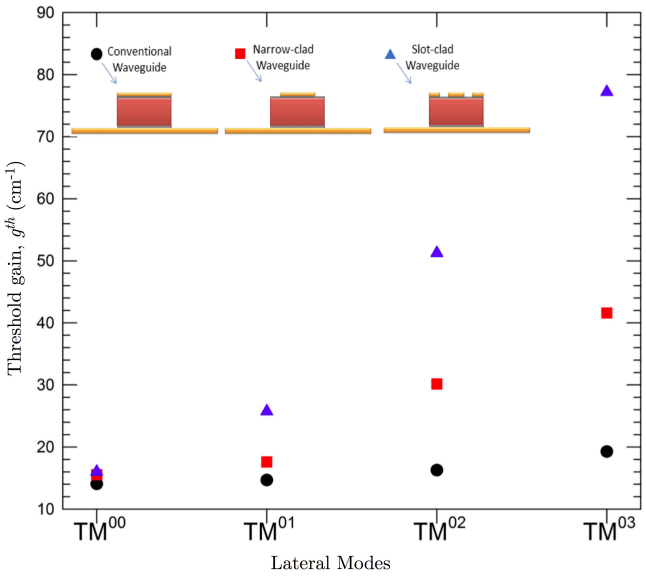

Fig. 7. Comparison of the threshold gain of the fundamental and lateral higher order modes in conventional, narrow-clad and slot-clad metal-metal waveguides. All three waveguides were compared at a ridge width of 200 μm. For the narrow clad waveguide, the width of the upper exposed n^+ GaAs was fixed at $\delta = 3.0$ μm. For the slot clad waveguide, the width of the outer metal layer W_1 and the slotted opening δ were taken to be 15.0 μm and 3.0 μm, respectively.

to be substantially higher for the slot clad waveguide. From the comparison of the waveguide structures shown in this figure, in a conventional waveguide, the g^{th} value of the TM^{01}, TM^{02} and TM^{03} modes are 2.9%, 3% and 13% higher than that of the fundamental TM^{00} mode, respectively. In a narrow-clad waveguide [7], the g^{th} values of the TM^{01}, TM^{02} and the TM^{03} modes are 17%, 49% and 100% higher than the fundamental TM^{00} mode, respectively. By contrast in a slot-clad waveguide, the g^{th} values of the TM^{01}, TM^{02} and TM^{03} modes are 1.5 times, 2.5 times and 4 times higher than the fundamental TM^{00} mode, respectively. It is evident from this figure that the slot-clad waveguide offers a better suppression of the higher-order lateral modes than does the narrow-clad waveguide [7].

VI. Conclusion

Higher order lateral modes in a THz QCL, based on metal-metal waveguides can degrade the beam quality of the device by producing multiple lobes in the far-field profile of the emitted beam. Such effects may have several undesirable consequences in many applications where it is critical to have a good beam profile from the source. It was shown previously by others that by reducing the width of the upper cladding layer of the QCL waveguide it is possible to raise the differential threshold gain between the fundamental and higher order modes. In an attempt to further advance the process of eliminating the higher-order lateral modes, a slot clad waveguide has been proposed here. The modal properties of this waveguide have been been simulated using a full vectorial **H** field based finite element method. Results obtained and presented here reveals that such a waveguide raises the differential threshold gain between the fundamental mode

and higher-order lateral modes by a greater margin than do previously reported designs of metal-metal QCL waveguides. Thus it can be inferred that the slot-clad waveguide is able to suppress the higher-order lateral modes better than previously reported designs.

REFERENCES

[1] R. Köhler, A. Tredicucci, F. Beltram, H. E. Beere, E.H. Linfield, A.G. Davies, D.A. Ritchie, R.C. Lotti and F. Rossi "Terahertz Semiconductor Heterostructure Laser," *Nature*, vol. 417, pp. 156–159, 2002.

[2] B. S. Williams, S. Kumar, H. Callebaut and Q. Hu "Terahertz Quantum Cascade Laser at $\lambda \sim 100$ μm using metal waveguide for mode confinement," *Appl. Phys. Lett.*, vol. 83, pp. 2124–2126, 2003.

[3] J. Ulrich, R. Zobl, N. Finger, K. Unterrainer, G. Strasser and E. Gornik, "Terahertz-electroluminescence in a quantum cascade structure," *Physica B*, vol. 272, pp. 216–218, 1999.

[4] B. S. Williams, S. Kumar, Q. Hu, and J. Reno, "High-power terahertz quantum-cascade lasers," *Electron Lett.*, vol. 42, pp. 89-91, 2006.

[5] M. A. Belkin, Q. J. Wang, C. Pflügll, A. Belyanin, S. P. Khanna, A. G. Davies, E. H. Linfield and F. Capasso "High-temperature operation of terahertz quantum cascade laser sources," *IEEE J. Sel. Topics Quantum Electron.*, vol. 15, pp. 952–967, 2009.

[6] A. J. L. Adam, I. Kašalynas, J. N. Hovenier, T. O. Klassen, J. R. Gao, E. E. Orlova, B. S. Williams, S. Kumar, Q. Hu and J. L. Reno"Beam pattern investigation of terahertz quantum cascade lasers," *Appl. Phys. Lett.* vol. 88, pp. 151105-1–151105-3, 2006.

[7] J. A. Fan, M. A. Belkin, F. Capasso, S. P. Khanna, M. Lachab, A. G. Davies and E. H. Linfield "Wide-ridge metal metal terahertz quantum cascade lasers with higher order lateral mode suppression," *Appl. Phys. Lett.* vol. 92, pp. 031106-1–031106-3, 2008.

[8] M. Geiser, C. Pflügl, A. Belyanin, Q. J. Wang, N. Yu, T. Edamura, M. Yamanishi, H. Kan, M. Fischer, A. Wittman, J. Faist and F. Capasso "Gain competition in dual wavelength quantum cascade lasers," *Opt. Express*, vol. 18, pp. 9900–9908, 2010.

[9] J. A. Fan, M. A. Belkin, F. Capasso, S. Khanna, M. Lachab, A. G. Davies and E. H. Linfield "Surface emitting terahertz quantum cascade laser with a double-metal waveguide," *Opt. Express*, vol. 14, pp. 11672–11680, 2006.

[10] A. W. M. Lee, Q. Qin, S. Kumar, B. S. Williams, Q. Hu and J. L. Reno "High power and high temperature THz quantum cascade lasers based on lens coupled metal-metal waveguides," *Opt. Lett.*, vol. 32, pp. 2840–2842, 2007.

[11] P. Gellie, W. Maineult, A. Andronico, G. Leo, C. Sirtori, S. Barbieri, Y. Chassagneux, J. R. Coudevylle, R. Colombelli, S. P. Khanna, E. H. Linfield and A. G. Davies "Effect of transverse mode structure on the far field pattern of metal-metal terahertz quantum cascade lasers," *J. Appl. Phys.*, vol. 104, pp. 124513-1–124513-3, 2008.

[12] S. Kohen, B. S. Williams and Q. Hu "Electromagnetic modeling of terahertz quantum cascade laser waveguides and resonators," *J. Appl. Phys.*, vol. 97, pp. 053106-1–053106-9, 2005.

[13] M. A. Ordal, L. L. Long, R. J. Bell, S. E. Bell, R. R. Bell, R. W. Alexander Jr., C. A. Ward, "Optical properties of the metals Al, Co, Cu, Au, Fe, Pb, Ni, Pd, Pt, Ag, Ti, and W in the infrared and far infrared," *Appl. Opt.*, vol. 22, pp. 1099–1119, 1983.

[14] B. M. A. Rahman and J. B. Davies "Finite-element analysis of optical and microwave waveguide problems," *IEEE Trans. Microw. Theory Tech.*, vol. 32, pp. 20–28, 1984.

[15] H. Tanvir, B. M. A. Rahman, N. Kejalakshmy, A. Agrawal and K. T. V. Grattan "Evolution of highly confined surface plasmon modes in terahertz quantum cascade laser waveguides," *J. Lightwave Technol.*, vol. 29, pp. 2116–2125, 2011.

Huda Tanvir (S'08) was born in Sylhet, Bangladesh. He graduated with a first class honours in BEng. Electrical and Electronic Engineering from City University London in 2006. He has recently been awarded the degree of Doctor of Philosophy (Ph.D) in Photonics at the School of Engineering and Mathematical Sciences, City University London. His research interest includes device characterisation of guided wave and plasmonic devices, particularly those operating at terahertz frequencies. Mr. Tanvir was awarded two prestigious scholarships from the International Society of Optical Engineering (SPIE) for his potential long range contribution in the field of photonics and optics. He was also ranked first in the Department of Electrical and Electronic Engineering, City University London, and was awarded the university prize for his achievement.

B.M.A Rahman (S'80-M'83-SM'94) received the B.Sc. Eng. and M.Sc. Eng. degrees (with distinctions) in electrical engineering from Bangladesh University of Engineering and Technology (BUET), Dhaka, Bangladesh, in 1976 and 1979, respectively, and the Ph.D. degree in electronics from University College London, London, U.K., in 1982. From 1976 to 1979, he was a Lecturer in the Department of Electrical Engineering, BUET. In 1982, he was a Postdoctoral Research Fellow at University College London, where he continued his research on the development of finite-element method for characterising optical guided wave devices. In 1988, he joined City University, London, as a Lecturer, where he is now a Professor, and leads the research group on photonics modelling, specialised in the use of rigorous and full-vectorial numerical approaches to design, analyse, and optimize a wide range of photonic devices, such as spot size converters, high speed optical modulators, compact bend designs, power splitters, polarization splitters, polarization rotators, polarization controllers, terahertz devices, etc. He is the author or coauthor of more than 400 journal and conference papers, and his journal papers have been cited more than 1800 times. Prof. Rahman received two gold medals for being the best undergraduate and graduate students of the university in 1976 and 1979, respectively. In 1979, he was awarded with a Commonwealth Scholarship to study for a Ph.D. degree in the U.K. He is a member of the Optical Society of America and the Institution of Engineering and Technology (U.K.). He is a Chartered Engineer, U.K.

K.T.V. Grattan received the B.S. degree in physics (first class hons.) and the Ph.D. degree from the Queens University, Belfast, U.K., in 1974 and 1978, respectively, and the D.Sc. degree from City University, London, U.K., in 1992. In 2002, he was a Postdoctoral Research Assistant at Imperial College, London, where he was engaged in research during on laser systems for photophysical systems investigations. His work in the field continued with research using ultraviolet and vacuum ultraviolet lasers for photolytic laser fusion driver systems and studies on the photophysics of atomic and molecular systems. In 1983, after five years at Imperial College, he joined City University, where he was involved in research on novel optical instrumentation, especially in fiber optic sensor development for physical and chemical sensing, was the Head of the Electrical, Electronic and Information Engineering Department from 1991 to 2001, and is currently the Dean of Engineering and Mathematical Sciences and of the School of Informatics. The work has led into several fields including luminescence based thermometry, Bragg grating based strain sensor systems, white light interferometry, optical system modelling and design, and optical sensors for environmental and structural health monitoring. He is the author of more than 700 papers and his work has been extensively published in the major journals and at international conferences. Prof. Grattan was a Chairman of the Applied Optics Division of the U.K. Institute of Physics and the President of the Institute of Measurement and Control in 2000. He was elected a Fellow of the Royal Academy of Engineering in 2008. He regularly has been an invited speaker at international conferences.